

Article

# A Cross-Medium Uplink Communication Model Merging Acoustic and Millimeter Waves

Yu Gai <sup>1</sup>, Qi Tan <sup>1</sup>, Yating Zhang <sup>1,\*</sup> , Zhengyi Zhao <sup>1</sup>, Yiguang Yang <sup>2</sup>, Yanyan Liu <sup>3</sup>, Ruitao Zhang <sup>4</sup> and Jianquan Yao <sup>1,2,\*</sup>

<sup>1</sup> School of Precision Instrument and Opto-Electronics Engineering, Tianjin University, Tianjin 300072, China; 2021202345@tju.edu.cn (Y.G.); 1023202030@tju.edu.cn (Q.T.); 1023202035@tju.edu.cn (Z.Z.)

<sup>2</sup> Laoshan Laboratory, Qingdao 266237, China; ygyang@qnlm.ac

<sup>3</sup> Science and Technology on Electro-Optical Information Security Control Laboratory, Tianjin 300308, China; lyy13@126.com

<sup>4</sup> Deepinfar Ocean Technology Inc., Tianjin 300457, China; ruitao.zhang@deepinfar.com

\* Correspondence: yating@tju.edu.cn (Y.Z.); jqyao@tju.edu.cn (J.Y.)

**Abstract:** Uplink communication across the water–air interface holds great potential for offshore oil surveys and military applications. Among the various methods available for implementing uplink communication, translational acoustic-RF (TARF) communication stands out due to its ability to withstand wave interference and exhibit low absorption losses. However, the physical processes underlying such systems are currently under-researched, and channel models for evaluating its communication performance indicators are lacking. Herein, we propose a signal-to-noise ratio (SNR) channel model for evaluating the performance metrics of an uplink communication system combining acoustic and millimeter waves for the first time and validate the accuracy of the proposed model through experiments. Specifically, in the process of model construction, the physical process of the communication system was deeply studied, and the corrections of multipath effects, box vibrations, and second-order nonlinear coefficients of the amplitude of the water surface were realized. The water-to-air cross-medium communication system was built, and communication experiments were conducted to validate the feasibility of combining acoustic and millimeter wave communication. This research provides a theoretical and experimental foundation for the design and evaluation of TARF communication systems, providing valuable guidance for enhancing the system's performance metrics and promising an innovative approach for modern seaborne communication.

**Keywords:** uplink communication; SNR channel model; acoustic and millimeter waves



**Citation:** Gai, Y.; Tan, Q.; Zhang, Y.; Zhao, Z.; Yang, Y.; Liu, Y.; Zhang, R.; Yao, J. A Cross-Medium Uplink Communication Model Merging Acoustic and Millimeter Waves. *J. Mar. Sci. Eng.* **2023**, *11*, 2102. <https://doi.org/10.3390/jmse11112102>

Academic Editors: Sergey Pereselkov, Matthias Ehrhardt, Pavel Petrov and Rafael Morales

Received: 25 September 2023

Revised: 16 October 2023

Accepted: 25 October 2023

Published: 2 November 2023



**Copyright:** © 2023 by the authors. Licensee MDPI, Basel, Switzerland. This article is an open access article distributed under the terms and conditions of the Creative Commons Attribution (CC BY) license (<https://creativecommons.org/licenses/by/4.0/>).

## 1. Introduction

Uplink communication across the water–air interface holds immense significance in the field of deep-sea exploration and submarine communications, garnering considerable attention [1–3]. A wide range of uplink communication methods exist, broadly classified into three categories [4]: relay-based communication [5–7], optical direct communication [8,9], and nonoptical direct communication [10–15]. Relay-based communication is susceptible to environmental and adverse weather conditions such as drift, currents, or surface waves [16]. Both optical and nonoptical wireless communications are often severely compromised by channel complexity and wave problems [17–20], and transmission is also vulnerable to significant interference arising from seawater absorption [21]. Overall, further research is needed to advance technologies pertaining to uplink communications across the water–air interface.

Fortunately, in 2018, Tonolini and Adib at MIT introduced translational acoustic-RF communication (TARF), a novel form of uplink wireless communication [22]. TARF combines the utilization of acoustic waves and millimeter waves, offering a promising approach to overcome the limitations and challenges associated with conventional communication

methods. TARF demonstrates the ability to achieve communication rates of up to 400 bps and maintain reliable communication even in the presence of the disturbances caused by water surface waves with amplitudes of up to 16 cm. Based on matching the frequency of surface waves to the acoustic signal of an underwater speaker, TARF exhibits resistance to water wave interference and ensures enhanced privacy. The system effectively addresses the challenges associated with underwater turbulence, air bubbles, and high absorption losses through the employment of hydroacoustic technology. Hence, TARF technology may become one of the preferred solutions in the field of cross-medium communication in the future. Further research is essential to delve into the intricacies of the TARF communication method, including system optimization and an in-depth understanding of its underlying physical processes.

In offshore oil exploration and military applications, translational acoustic-RF communication (TARF) technology exhibits significant application potential. For instance, in offshore oil exploration applications, by analyzing the water surface waves generated by acoustic signals sent from underwater robots to the water surface, TARF technology assists in more accurately locating oil well positions and the real-time monitoring of the seabed environment to ensure the safety of personnel and equipment. In military applications, submarines can emit modulated acoustic waves to the water surface, which are then decoded by aircraft, enabling cross-medium communication between submarines and aircraft, ensuring communication safety and concealment. However, we also acknowledge that there are some common limitations and challenges faced by TARF technology in real-world applications, including depth, multipath effects caused by environmental factors, wind and waves, hardware requirements, real-time performance, and the communication rate. These factors may affect the effectiveness and application range of TARF technology. Further research and technological optimization are needed to promote the application of TARF technology in these critical areas and overcome these limitations and challenges.

Model building is an effective approach for understanding physical processes and communication systems [23,24]. In the context of surface wave modeling in water, significant contributions were made by Lagrange, who derived a linear control equation for small amplitude wave theory. This was further explored by Cauchy and Poisson, who investigated the initial value problem associated with the general linear water wave equation. In 2020, the Ocean College of Zhejiang University developed an end-to-end channel theoretical model based on linear microamplitude wave theory, which was validated through low-frequency experiments [25]. However, despite some progress being made in the investigation of this communication system, the physical processes of the system remain relatively understudied, and there is a notable absence of a corresponding channel model for assessing its communication performance metrics.

In this paper, a signal-to-noise ratio (SNR) channel model for evaluating the performance metrics of communication systems was successfully constructed, which was rigorously validated through experimental verification.

The main contributions of this paper can be summarized as follows:

- (1) The SNR channel model of TARF was proposed for the first time, and the corrections for multipath effects, box vibrations, and a second-order nonlinear coefficient for amplitudes of the water surface wave were completed;
- (2) The experimental validation of the SNR ratio channel model was conducted;
- (3) A water-to-air cross-medium communication system was constructed, and a series of experiments were conducted.

The remainder of this paper is structured as follows: Section 2 provides a comprehensive exposition of the physical process of bridging acoustic waves and millimeter waves. It elaborates on the construction of the SNR channel model and presents the experimental validation. In Section 3, a series of communication experiments are described, along with the proposal of a stable and effective filtering algorithm. Furthermore, the utilization of a sliding Fourier transform approach to mitigate intercode errors is elucidated.

Section 4 concludes the paper by summarizing the key findings and discusses the scope for future work.

## 2. Model of Cross-Medium Communication Channel

In order to achieve water-to-air cross-medium communication, it is imperative to establish a comprehensive communication channel model as a foundational step. By leveraging the distinctive features of the constructed channel model, one can flexibly opt for appropriate carrier frequencies and modulation methods. By proactively assessing and predicting the communication metrics, a water-to-air cross-medium communication system can be constructed to precisely cater to the specified SNR and transmission distance requirements.

The analysis of physical processes is widely recognized as a crucial component in engineering modeling. As depicted in Figure 1, water-to-air cross-medium communication entails three main parts: the underwater channel, the water–air interface, and the air channel. In the underwater channel, the speaker emits an acoustic signal, propagating as a pressure wave from the underwater environment towards the water surface. At the air–water interface, the acoustic signal propagating to the water surface induces the formation of water surface waves due to the mechanical characteristics of the pressure waves. By employing millimeter wave radar (MMWR) in the air channel, it becomes feasible to detect the surface waves and subsequently acquire the transmitted information from the speaker.

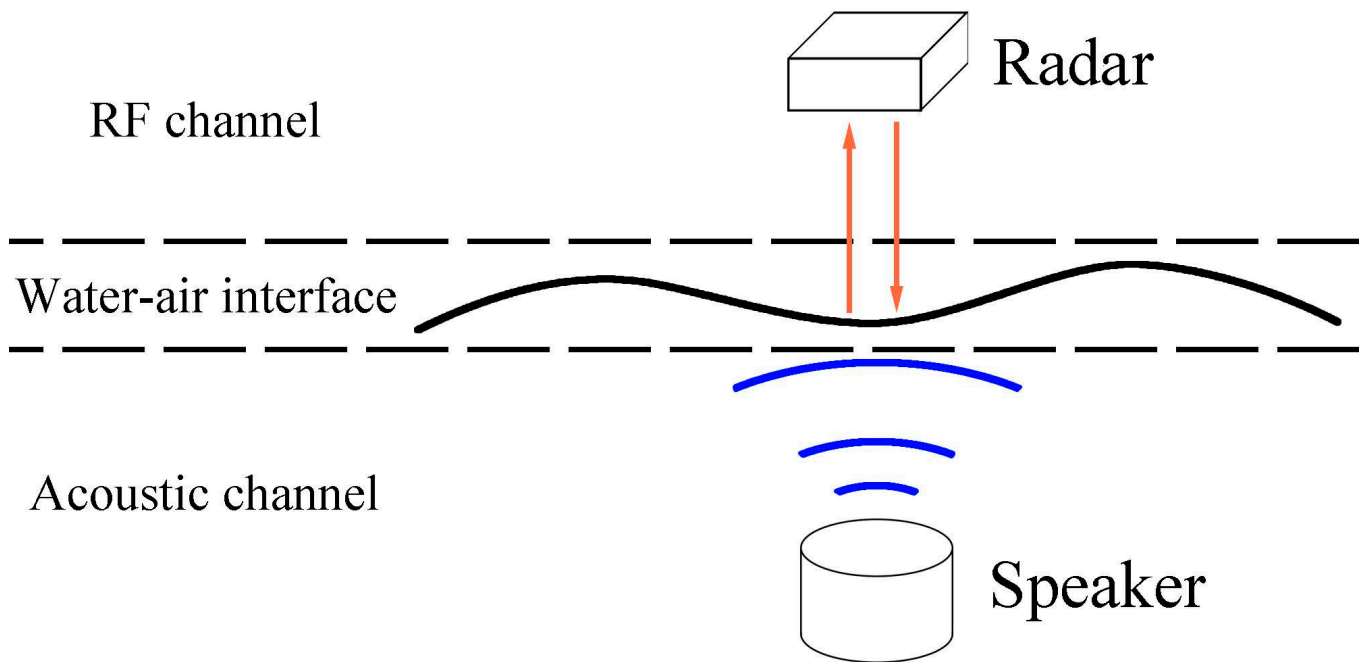


**Figure 1.** Schematic of the signal propagation process in cross-medium communication.

### 2.1. Physical Process

#### 2.1.1. Underwater Propagation of Acoustic Signals

During transmission, the acoustic signal emitted by speaker under water undergoes gradual attenuation. Underwater acoustic waves experience two primary types of attenuation: diffusion attenuation and absorption attenuation. Diffusion attenuation arises from the expansion of the wavefront surface with distance, leading to propagation loss that follows the inverse square law  $1/r^2$ . Absorption attenuation stems from seawater absorption and inhomogeneity scattering, resulting in propagation loss that adheres to the exponential law  $e^{-\alpha r}$ . Combined, these laws can be summarized as follows [22]:

$$A(r, f) = \frac{A_0(f)e^{-\alpha r}}{r} \tag{1}$$

where  $A_0$  represents the initial peak value of the underwater acoustic source,  $r$  denotes the underwater transmission distance of the acoustic source signal,  $f$  corresponds to the frequency of the acoustic source signal,  $A(r, f)$  indicates the amplitude of the acoustic source signal after traveling the underwater distance  $r$ , and  $\alpha$  represents the attenuation coefficient of the acoustic source signal in the water. The definition of  $\alpha$  is presented below [26]:

$$\alpha(r) = \left( \frac{0.109f^2}{1 + f^2} + \frac{40.7f^2}{4100 + f^2} + 3.01 \times 10^{-4}f^2 \right) \times \left( 1 - 6.67 \times 10^{-5}r \right) \times 10^{-6} \quad (2)$$

The underwater acoustic source signal propagates through water as a pressure wave. For calculation, the acoustic signal amplitude can be converted into sound pressure using the following equation [27].

$$p_i(f, r, t) = A(r, f)e^{jf(t - \frac{r}{v})} \quad (3)$$

where  $p_i$  represents the incident sound pressure, and  $v$  is the sound speed, which is affected by many underwater environmental parameters. The specific relationship is as follows [26]:

$$v = 1450 + 4.21TEM - 0.037TEM^2 + 1.14(S - 35) + 0.175P_w \quad (4)$$

where  $TEM$  is the temperature,  $S$  stands for salinity, and  $P_w$  represents water pressure.

### 2.1.2. Acoustically Induced Surface Waves

The acoustic signal, when propagated to the water surface, induces water surface waves. This physical process can be mathematically modeled by linearizing the universal hydrodynamic equations based on the linear small amplitude wave theory. It describes the acoustic pressure-induced transverse microamplitude waves on the water surface, and the 3D mathematical model is represented by Equation (5) [27]:

$$\delta(x, y, t) = \frac{2p_i}{\omega\rho v} e^{-\alpha\sqrt{x^2+y^2}} \cos\left(k\sqrt{x^2+y^2} - 2\pi ft\right) \quad (5)$$

where  $p_i$  is the underwater sound source pressure,  $\rho$  is the density of water,  $v$  is the speed of sound, and  $x$  and  $y$  are the coordinates on the horizontal plane, respectively.

### 2.1.3. Detection of Water Surface Wave by MMWR

Above the water surface, a radar transmits frequency modulated continuous waves (FMCW) for measuring the amplitudes of the surface wave. The transmitted signal from the radar is mixed with the received signal to generate an intermediate frequency signal (IF Signal). The phase of the IF signal is utilized to reconstruct the vibration waveform of the surface wave. The relationship between the received phase of the radar and the amplitude of a surface wave is described by the following equation [22]:

$$\Delta\varphi_{MMWR}(t) = 4\pi \frac{\delta(t)}{\lambda} \quad (6)$$

In this equation,  $\delta(t)$  represents the microamplitude of a surface wave, and  $\lambda$  denotes the wavelength of the radar transmitted signal. By performing the unwrapping process, the waveform and the true amplitude of the water surface can be restored.

## 2.2. Model Adjustments and Analysis

### 2.2.1. Multipath Fading Correction

Multipath fading occurs when acoustic waves encounter various propagation paths in water, such as direct, reflected, and scattered paths, leading to signal interference at the receiving end. In our experimental condition, the short transmission distance and relatively

small time delay expansion result in narrowband fading, where only a random process reflecting a random amplitude and phase is added during the merging of multipath signals.

Due to the close transmission distance, multipath fading caused by the reflection of acoustic waves cannot be ignored, leading to an interference effect on the sound pressure at the water–air interface.

In the experimental conditions, multipath fading was observed along two main paths, as depicted in Figure 2. One (Path 1) involved the vertical reflection of acoustic waves from the water surface to the speaker, followed by another vertical reflection from the speaker back to the water surface, resulting in multipath fading. The other (Path 2) was caused by the reflection of acoustic waves from the wall of the water tank covered with silencing cotton, resulting in multipath fading at the water–air interface.

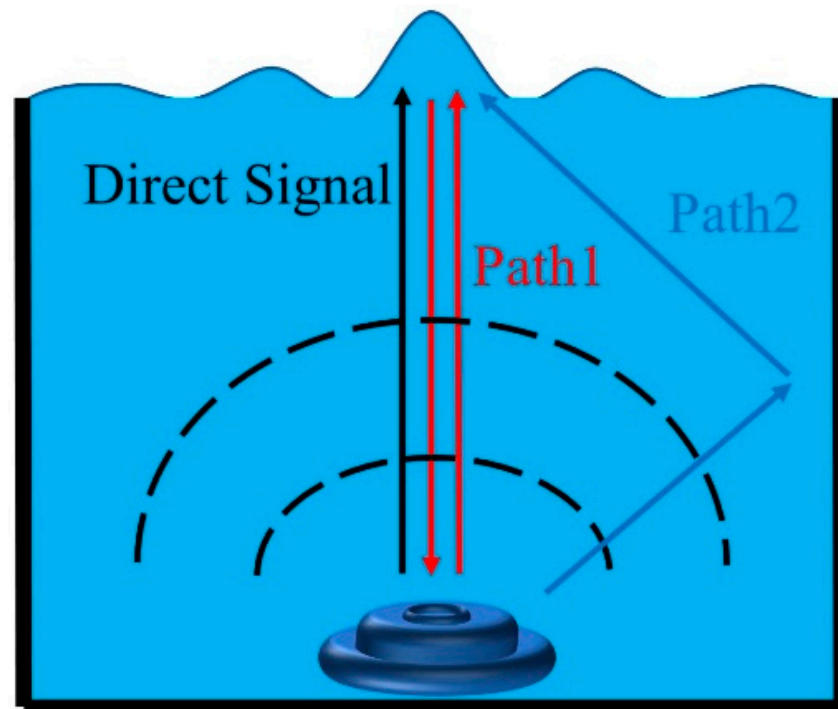


**Figure 2.** Multipath fading under experimental conditions.

Correcting for narrowband fading caused by multiple paths was not considered in the physical process; thus, a correction coefficient  $\zeta$  was added to the sound pressure at water surface. The correction equation is as follows:

$$\delta_1 = \zeta\delta_0 \tag{7}$$

### 2.2.2. Background Noise Target Component Correction

Despite the placement of the speaker at the bottom of the tank and the use of silencing cotton, the vibration remained unavoidable. This vibration at the water–air interface introduced a noise component at the target frequency, which affected the accurate calculation of the SNR. To address this, a correction coefficient  $\varepsilon$  was introduced to the signal energy. The formal representation of this correction is as follows:

$$E = E_S + \varepsilon \tag{8}$$

### 2.2.3. Second-Order Nonlinear Correction

The modeling of water surface waves involves fluctuation theory, which encompasses both linear and nonlinear approaches. In linear fluctuation theory, it is typically assumed that the fluctuations have a small amplitude, resulting in a negligible wave steepness.

Higher-order terms in the wave equation can be disregarded, and only first-order terms are considered. Equation (5) represents a model of microamplitude waves at the water surface, derived using linear fluctuation theory. It is commonly accepted that fluctuations at the submicron level can be referred to as microamplitude waves.

However, in the current experimental setting, characterized by a shallow water depth and high sound pressure level, the amplitude of surface waves could reach several hundred micrometers, leading to a significant wave steepness. In this scenario, the microamplitude wave model derived from linear fluctuation theory was no longer suitable. To correct this, we introduced a quadratic correction coefficient  $\eta p_i^2$  to the amplitude of the water surface, which can be expressed by the following correction formula:

$$\delta_0(\eta) = \delta + \eta p_i^2 \tag{9}$$

### 2.3. SNR Model

The initial step was to capture background noise information. Since waves possess mechanical properties, they can be viewed as structural disturbances under similar conditions. As a result, the background noise could be collected in advance and incorporated into the model as additive noise  $N(t)$ . To assess the total energy  $E_N$  of the background noise, a Fourier transform was applied to  $N(t)$  and a spectral analysis was conducted.

$$F(\omega) = \int_{-\infty}^{\infty} N(t)e^{-j\omega t} dt \tag{10}$$

$$E = \sum F(\omega) \tag{11}$$

The acoustic signal emitted by the speaker was a single-frequency signal. As observed in [28], a significant amplitude was only observed in water surface waves with the same frequency as the vibrating point source. The energy of the surface wave can be derived from the energy of a single-frequency signal using the following formula:

$$E_s = \frac{1}{2} \delta^2 T \tag{12}$$

where  $T$  is the time of acquisition, and the expression for SNR is deduced as:

$$SNR = 10 \lg \left( \frac{P_s}{P_n} \right) \tag{13}$$

$$SNR = 10 \lg \left( \frac{\zeta^2 \left( \frac{2p_i}{\omega \rho v} + \eta p_i^2 \right)^2 T + 2\varepsilon}{2E_N} \right) \tag{14}$$

where  $P_s$  stands for the power of the signal and  $P_n$  is the power of the noise. By substituting the system parameters into the SNR calculation Formula (13), we can derive the SNR model as expressed in Formula (14). In addition,  $\zeta$  represents the correction coefficient for underwater acoustic interference caused by underwater multipath attenuation;  $\varepsilon$  denotes the correction coefficient for the signal gain resulting from the energy component of the box vibration at the target frequency, which is very small;  $\eta$  is the nonlinear correction coefficient for the linear fluctuation theory.

In constructing this model, some fundamental assumptions were made. We assumed that the water surface waves collected by the radar were accurate and unaffected by other interference factors. Moreover, we assumed that the underwater acoustic waves were transmitted in the form of spherical waves, aiding in simplifying the model and enhancing the accuracy of predictions. This channel model differs significantly from existing models in several key aspects. By introducing correction coefficients, our model optimized the influence of environmental factors to accurately reflect the actual communication environment. Unlike the linear waveforms commonly used in existing models, we carried out

nonlinear optimization on the waveforms of the water surface waves, aiding in describing and predicting communication performance more accurately. Through these optimizations, our model is capable of providing more intuitive and practical communication performance metrics, offering valuable references for practical applications.

#### 2.4. Verification of Cross-Medium Communication Channel Model

A water-to-air cross-medium communication system was constructed to validate the model’s accuracy. The equipment and system diagrams are depicted in Figure 3. A single frequency acoustic signal was emitted underwater from a UW:30 speaker. The surface waves, triggered by the acoustic signal propagating to the water surface, were detected using the AWR1642 mm wave radar board provided by TI. The inside of the metal box containing the water and the power cable of the speaker were silenced using silencer cotton, which minimized the impact of external sound, the box, multipath interference, and the vibration of the power cable at the water surface.

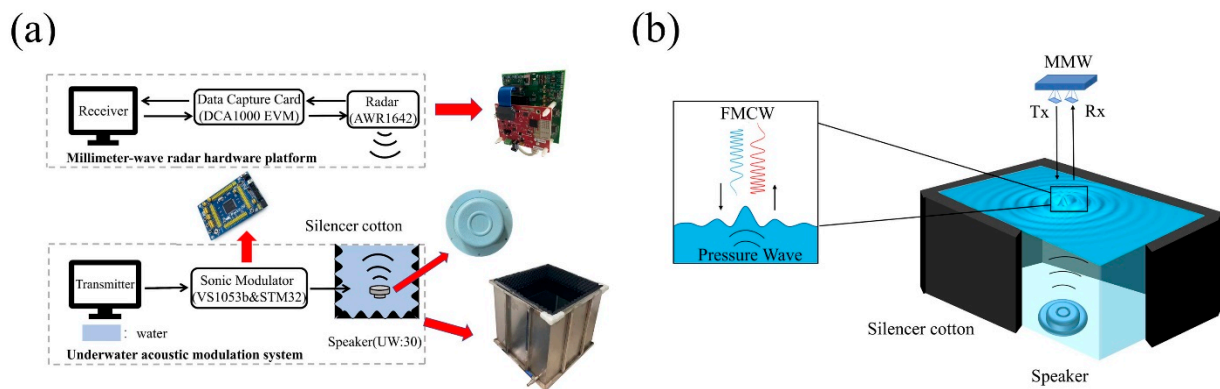


**Figure 3.** Water-to-air cross-medium communication system based on MMWR. (a) Equipment diagram. (b) System diagram.

##### 2.4.1. Noise Test at Silent Source

Initially, the background noise  $N(t)$  in the system needed to be measured as an additive component. This noise served as background noise for the model and its measurement was crucial for an accurate analysis. To capture the time-domain signal of the noise, the waveform of the water surface waves can be recorded using MMWR. This should be done with the speaker, which was energized but did not emit any acoustic signals. However, solely analyzing the time domain signal was insufficient for understanding the noise characteristics. A spectral analysis was necessary to gain further insights into its properties. The obtained test results are presented in Figure 4.

Based on our measurements, the following conclusions can be drawn. In the time domain, the maximum value of the surface wave amplitude in 5 s is  $45 \mu\text{m}$ . In the absence of an acoustic signal, the amplitude of the surface wave reaches the micron level. The influence of the environment on water–air cross-medium communication cannot be overlooked. In the frequency domain, noise energy predominantly resides in the low-frequency range from 0 Hz to 45 Hz. To minimize the impact of noise, it is advisable to avoid utilizing this frequency band for information transmission. Consequently, for effective communication, a carrier frequency of at least 100 Hz is necessary. To mitigate noise interference on the transmitted signal and enhance communication quality and stability, it is recommended to configure the filter with a low cut-off frequency of 100 Hz.

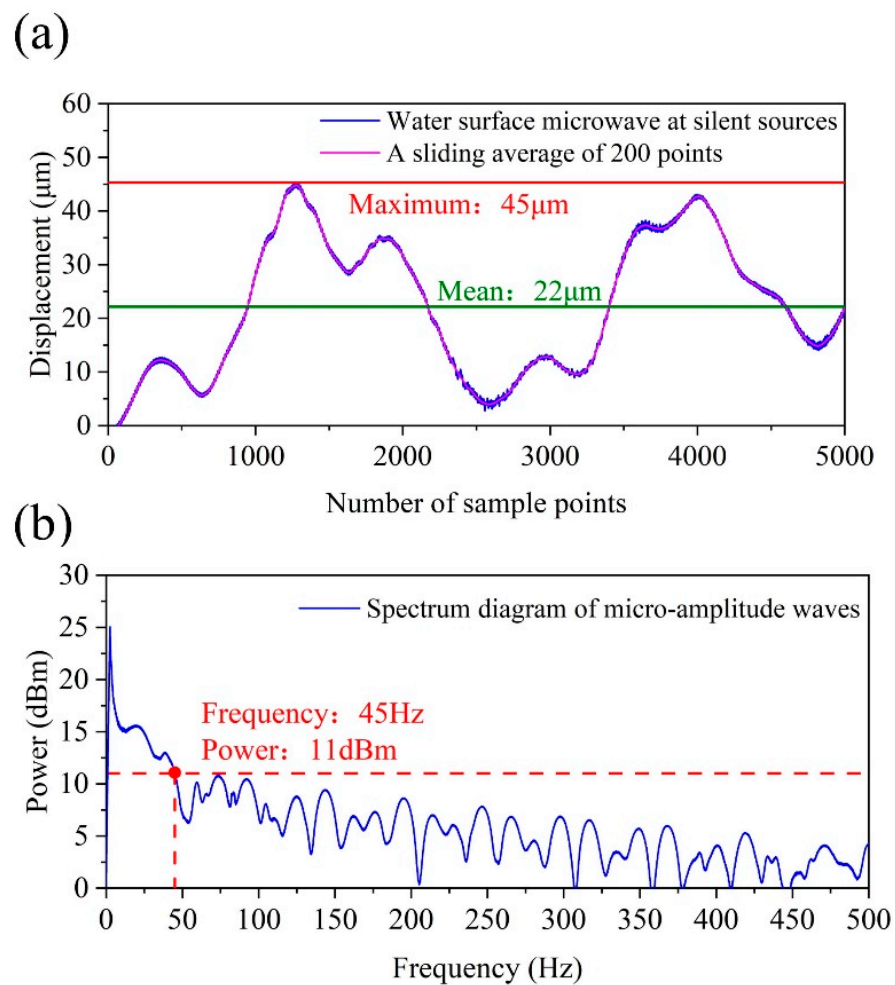


**Figure 4.** Analysis of noise at the silent source. (a) Time domain diagram. (b) Frequency domain diagram.

#### 2.4.2. SNR under Different Water Depths with an Acoustic Signal

Water surface waves produced by an acoustic signal with a frequency of 146 Hz were detected within the depth range from 10 cm to 60 cm. The sampling interval was set at 5 cm, and the experiment needed to be repeated four times for each group. Figure 5 displays the time domain and frequency domain plots of the surface waves when the water depth was 20 cm. The measured results indicate an SNR of 1.7 dB. Although the SNR value appears low, a distinct peak is clearly observable in Figure 5 following the Fourier transformation. The utilization of peak extraction allowed for effective information decoding, thereby demonstrating the efficacy of the communication model even under lower SNR conditions.

The SNR values were measured at different water depths in multiple experiments are shown in Figure 6. Measured data are visualized as red dots, while the model solution is represented by blue lines. Under the premise of water surface waves at the hundred-micron level, applying the model from Equation (5) directly, the calculated amplitude value differs from the actual value by three orders of magnitude, as this model was established under linear microamplitude wave conditions. Through nonlinear correction and environmental factor adjustments, our model achieved a high degree of correlation with the experimental data. The coefficient of determination, which quantifies the agreement between the measured data and the model calculations, was 0.982. This high  $R^2$  value significantly underscores the strong correlation between the observed data and the model predictions, showcasing the robustness and accuracy of our model in simulating the real-world scenario. In the results, the correction coefficient for multipath attenuation,  $\zeta$ , was determined to be 1.267 in the modeling equation. The energy correction coefficient for

the box vibration,  $\varepsilon$ , was determined to be  $2.607 \times 10^{-14}$ . The correction coefficient for second-order nonlinearity,  $\eta$ , was determined to be  $2.234 \times 10^{-10}$ . This indicates that the measured results were in high agreement with the model, verifying that the model we built demonstrates high reliability and predictive capability.

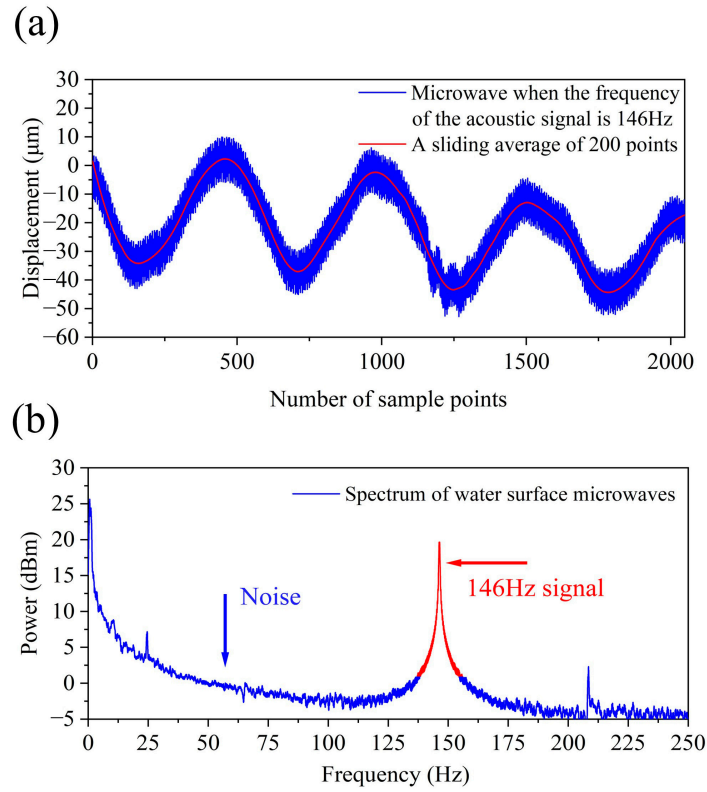


Figure 5. Surface wave in a water depth of 20cm with acoustic signal. (a) Time domain diagram. (b) Frequency domain diagram.

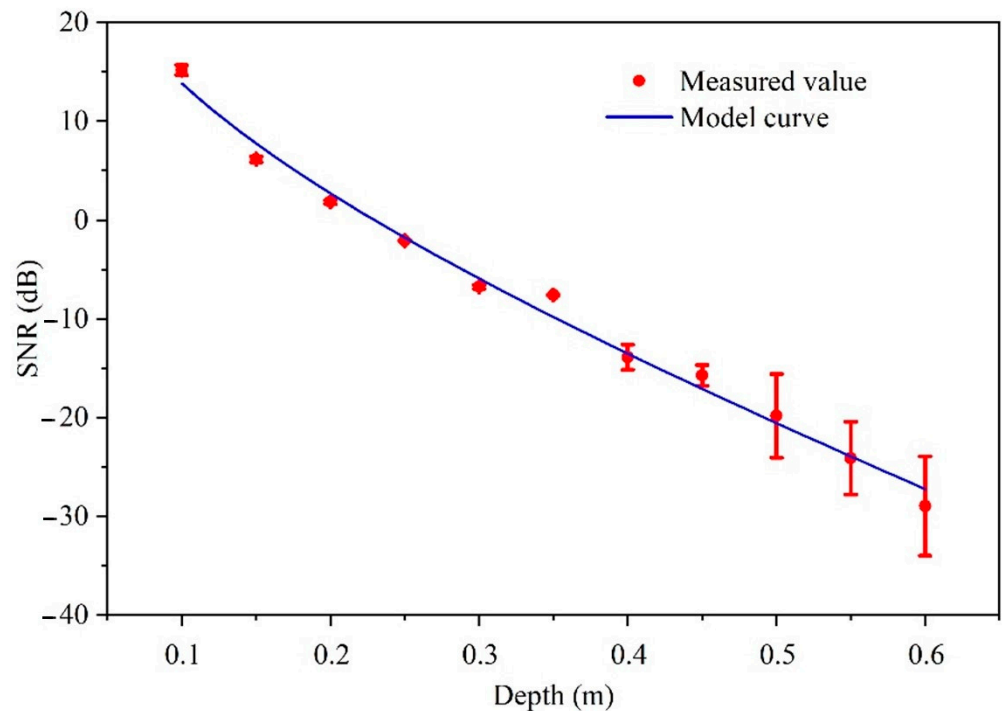


Figure 6. Test results of SNR changing with water depth and model curve.

In general scenarios, obtaining these coefficients necessitates model fitting. During model fitting, it is imperative to accurately constrain the range of correction coefficients based on the specific experimental conditions to ensure the authenticity and reliability of the coefficients. The range of correction factors based on our experimental conditions, hardware facilities, and identified sources of error is shown in Table 1 below. This required multiple iterations of calculations to find the optimal correction coefficient values that suited the experimental conditions.

**Table 1.** The value range of correction parameters.

$\zeta$	$\epsilon$	$\eta$
1~1.56	$10^{-14}$ ~ $10^{-15}$	$10^{-10}$ ~ $10^{-9}$

According to the experimental results cited in reference [22], it is observed that the amplitude of the surface wave decreased significantly when the frequency exceeded 300 Hz. This reduction in amplitude can have a negative impact on communication quality and lead to an increase in the bit error rate (BER). In order to achieve higher quality cross-medium communication, it is recommended to use a carrier frequency below 300 Hz. Additionally, setting the high cut-off frequency of the filter to 300 Hz will help ensure a better communication performance.

### 3. Communication

To validate the feasibility of combining acoustic and millimeter wave communication, a series of communication experiments were conducted using the TARF communication system.

#### 3.1. Coding Experiment

The interference-resistant 2-Frequency shift keying (2FSK) modulation technique was selected for the uplink communication across the water–air interface. In this modulation scheme, we used 146 Hz and 243 Hz as the underwater sources to represent binary “0” and “1”, respectively. To determine when the code elements were sent, a data encoding unit was employed, consisting of two start bits, eight data bits, one parity bit, and one stop bit. The data bits were encoded using ASCII codes as a reference. For instance, the letter “T” was encoded as “0001010011”.

##### 3.1.1. Band Pass Filter Design

To mitigate the interference caused by additive noise during the demodulation process, a filter was designed to suppress the noise. In this study, a 7th order Butterworth bandpass filter was employed due to its smooth frequency response and absence of phase distortion. The filter was configured with high and low cut-off frequencies set at 300 Hz and 100 Hz, respectively. This allows for the precise analysis of wave characteristics and accurate extraction of phase information from water surface fluctuations. The filtering results are presented below.

In aquatic environments, the noise primarily manifests as a superposition of  $1/f$  noise and white noise. Under the environmental conditions of our study, the attenuation rate stood at  $-8.07$  dB/decade, highlighting that the noise power predominantly resided in the low-frequency range. Given the severe attenuation of high-frequency acoustic waves in water and the relatively proximate transmission distance in our setup, it was impractical to indefinitely escalate the frequency of the acoustic waves in the communication system solely to circumvent low-frequency noise. Tailored to the carrier frequency range employed in our experimental system, we endeavored to elevate the low cut-off frequency of the filter without compromising the carrier, while retaining the narrowness of the transition band, leading to the successful design of the filter in question.

As depicted in Figure 7, the resulting filtered time domain image exhibits a smoother and clearer waveform. This effective noise reduction technique significantly diminished the influence of noise and interference. The filtering process played a crucial role in subsequent tasks, such as the waveform analysis and phase extraction of the water surface, thereby greatly enhancing the overall communication performance of the system.

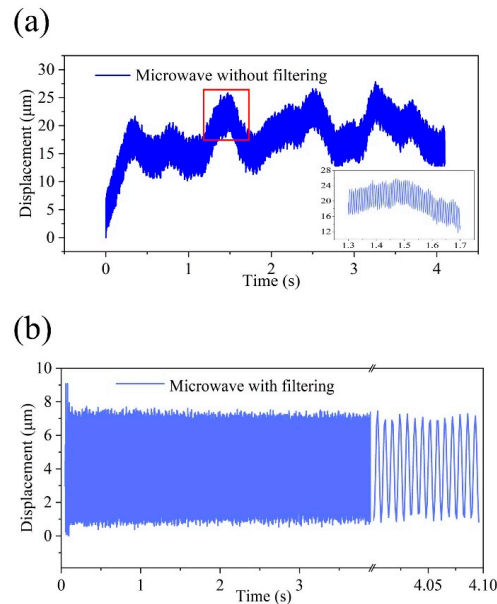


Figure 7. Comparison before and after filtering. (a) Before filtering. (b) After filtering.

### 3.1.2. Design of Acquisition and Demodulation Module

To ensure the precise transmission of information, we devised the acquisition and decoding algorithm illustrated in Figure 8. For modulation, each code element was assigned a duration of 1s. On the acquisition side, the MMWR operated at a sampling rate of 1 kHz, enabling 1000 samples per code element. The demodulation algorithm was constructed based on the FMCW principle, with multichirp values being averaged. Subsequently, a one-dimensional FFT was applied, yielding a time-domain image.

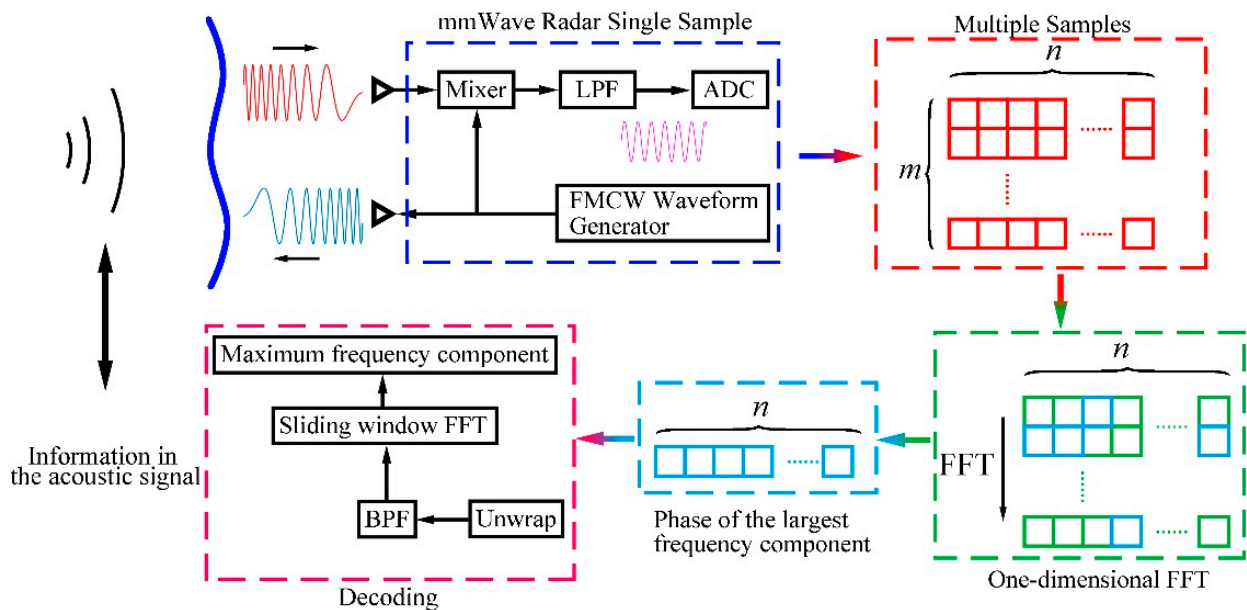


Figure 8. Schematic diagram of demodulation algorithm of water-to-air cross-medium communication system.

Following the filtering procedure, the time-domain waveform of the water surface wave generated by acoustic excitation was obtained. Subsequently, the filtered signal underwent a sliding window FFT with a window size of 256. The sliding window FFT is well-suited for real-time signal processing and spectral analysis. This approach allowed for the elimination of switching noise interference caused by speaker frequency switching, the precise detection and correction of intersymbol errors, and the real-time output of the surface wave spectrum. From the spectrum, the peak frequency component was extracted and output. A high output corresponds to 243 Hz, while a low output corresponds to 146 Hz. This process not only satisfies the frequency resolution of a single FFT but also enables the accurate differentiation of individual code elements.

### 3.1.3. Validation Test

The operator interface on the host computer was utilized to input and configure the encoded information. After the acquisition process was finished, the encoded characters “T”, “J”, and “U” were decoded on the acquisition side, employing the described algorithm and sliding window FFT. The decoding outcomes are depicted in Figure 9.

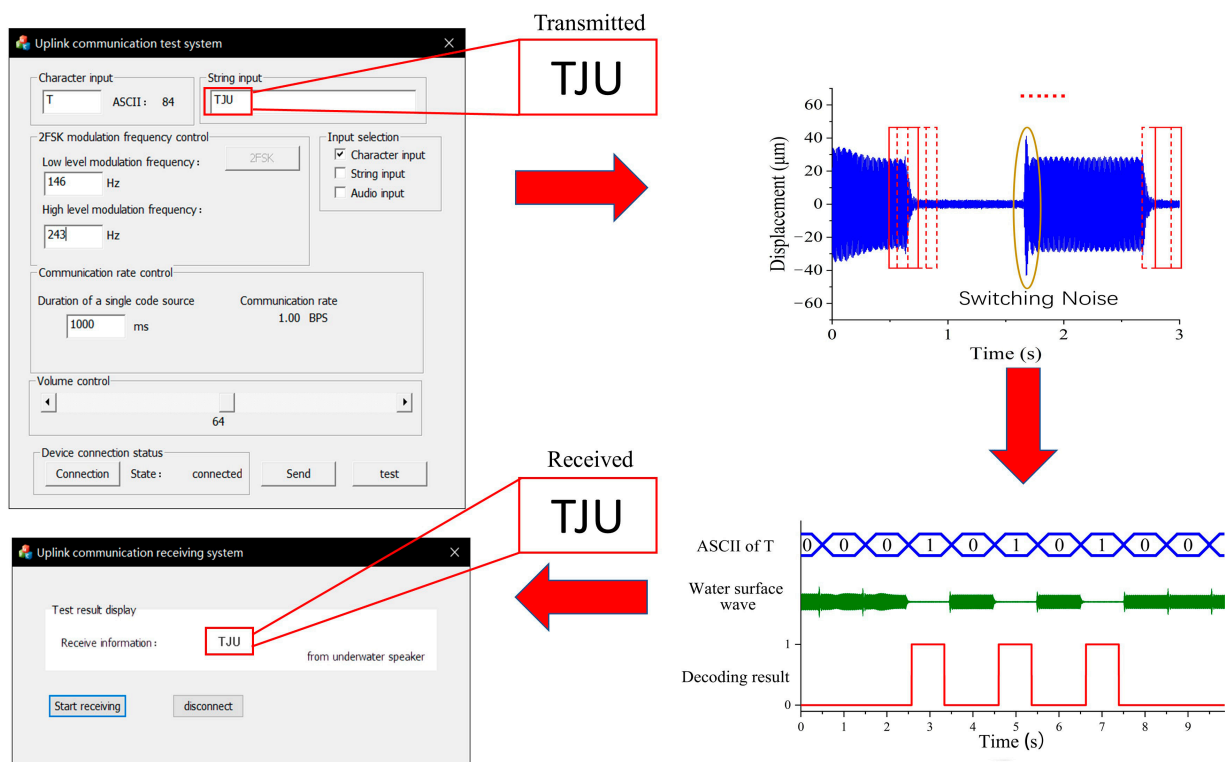


Figure 9. Decoding experiment results.

The experimental results demonstrate the favorable performance and feasibility of the TARF communication system utilizing frequencies of 146 Hz and 243 Hz. The amplitudes of the surface waves generated by acoustic signals of different frequencies exhibit significant variations, allowing for easy observation and distinction. This indicates that, by selecting an appropriate carrier frequency, efficient signal transmission can be achieved in the underwater environment, thereby providing an effective solution for water–air cross-medium communication.

## 4. Conclusions

In conclusion, we introduced a novel SNR channel model for evaluating the performance of the TARF communication system based on the amplitude characteristics observed in experimental conditions. We successfully corrected the original submicron level mi-

croamplitude wave model to a water surface amplitude model suitable for our experimental conditions through second-order nonlinear correction, and incorporated environmental factor corrections for box vibration and multipath effects. To obtain a more accurate and universal TARF channel model, there is an urgent need to develop a sound-induced water surface wave model that can accommodate a variety of nonlinear wave conditions, such as microamplitude and finite amplitude waves, which will be the foundation and key to constructing the TARF channel model. The proposed model was validated through experimental results, demonstrating a high correlation coefficient of 0.982. This high degree of correlation validates the effectiveness of the model and instills confidence in its applicability for analyzing and optimizing the communication performance in cross-medium uplink communication. Furthermore, a real-time water–air cross-medium communication system was developed, and communication experiments were conducted. Filtering and demodulation algorithms were designed to facilitate signal processing. The sliding Fourier transform method was applied to address issues such as speaker switching noise interference and intercode errors. Ultimately, the study achieved water–air cross-medium communication by combining acoustic and millimeter waves. The successful realization of water–air cross-medium communications merging acoustic and millimeter waves demonstrates the feasibility of the TARF communication system, unfurling promising horizons for ensuing research and progression. By thoroughly examining the amplitude characteristics and the corresponding SNR, the constructed model emerges as a pivotal tool for establishing the TARF uplink communication system. It aids in devising more robust and more efficient communication systems, propelling the advancement of water–air communication technology.

In upcoming sea trials, we aim to broaden the applicability of the TARF communication system in deep-water environments through several technical upgrades. Initially, addressing deep-water communication needs, we will replace existing loudspeakers with high-power acoustic transducers for clearer, more stable signal transmission in deeper waters, and employ higher resolution millimeter-wave radars to extend the maximum transmissible distance. Additionally, we plan to utilize efficient modulation techniques to enhance communication rates and system scalability. As the transmission distance and depth increase, we aim to develop more comprehensive channel models to accommodate varied application scenarios.

Subsequently, we will select suitable sea areas for trials, conducting them aboard vessels on the appointed day. We will place upgraded acoustic transducers at deeper locations, emitting preset acoustic signals, and use high-resolution radar systems on the water surface to monitor water surface fluctuations caused by acoustic signals in real time to decode the original information. The collected data will help assess the signal-to-noise ratio to measure the communication quality and stability and provide valuable insights for constructing and validating channel models for deeper waters. However, we recognize that TARF technology's scalability is affected by inherent limitations like multipath effects due to environmental conditions, severe high-frequency signal attenuation underwater, and susceptibility to wind and waves. We anticipate that data from sea trials will offer insights into these limitations, aiding in identifying technical solutions to optimize TARF technology in future research.

**Author Contributions:** Conceptualization, Y.G. and Q.T.; methodology, Y.G. and Y.Z.; software, Y.G.; validation, Y.G. and Z.Z.; formal analysis, Y.G., Q.T. and Y.Y.; Data Curation, Y.L. and Z.Z.; resources, R.Z.; writing—original draft preparation, Y.G.; writing—review and editing, Y.G. and Q.T.; visualization, Y.G.; supervision, J.Y.; project administration, Y.Z. and J.Y.; funding acquisition, J.Y. All authors have read and agreed to the published version of the manuscript.

**Funding:** This work was supported by the National Key Research and Development Program of China (2021YFB2800703), National Natural Science Foundation of China (U22A2008), Laboratory Foundation, and Laoshan Laboratory Science and Technology Innovation Project (No. LSKJ202200801).

**Institutional Review Board Statement:** Not applicable.

**Informed Consent Statement:** Not applicable.

**Data Availability Statement:** Data are contained within the article.

**Conflicts of Interest:** The authors declare no conflict of interest.

## References

1. Khan, M.A.; Alzahrani, B.A.; Barnawi, A.; Al-Barakati, A.; Irshad, A.; Chaudhry, S.A. A resource friendly authentication scheme for space-air-ground-sea integrated Maritime Communication Network. *Ocean. Eng.* **2022**, *250*, 110894. [[CrossRef](#)]
2. Kong, M.; Kang, C.H.; Alkhazragi, O.; Sun, X.; Guo, Y.; Sait, M.; Holguin-Lerma, J.A.; Ng, T.K.; Ooi, B.S. Survey of energy-autonomous solar cell receivers for satellite-air-ground-ocean optical wireless communication. *Prog. Quantum Electron.* **2020**, *74*, 100300. [[CrossRef](#)]
3. Akyildiz, I.F.; Pompili, D.; Melodia, T. Underwater acoustic sensor networks: Research challenges. *Ad Hoc Netw.* **2005**, *3*, 257–279. [[CrossRef](#)]
4. Luo, H.; Wang, J.; Bu, F.; Ruby, R.; Wu, K.; Guo, Z. Recent Progress of Air/Water Cross-Boundary Communications for Underwater Sensor Networks: A Review. *IEEE Sens. J.* **2022**, *22*, 8360–8382. [[CrossRef](#)]
5. Chen, H.; Chen, H.; Zhang, Y.; Xu, W. Decentralized estimation of ocean current field using underwater acoustic sensor networks. *J. Acoust. Soc. Am.* **2021**, *149*, 3106–3121. [[CrossRef](#)]
6. Thompson, F.; Guihen, D. Review of mission planning for autonomous marine vehicle fleets. *J. Field Robot.* **2019**, *36*, 333–354. [[CrossRef](#)]
7. Carlucho, I.; De Paula, M.; Wang, S.; Menna, B.V.; Petillot, Y.R.; Acosta, G.G. AUV position tracking control using end-to-end deep reinforcement learning. In Proceedings of the Oceans MTS/IEEE, Charleston, SC, USA, 22–25 October 2018; pp. 1–8.
8. Carver, C.J.; Tian, Z.; Zhang, H.; Odame, K.M.; QuattriniLi, A.; Zhou, X. Amphilight: Direct air-water communication with laser light. In Proceedings of the 17th USENIX Symposium on Networked Systems Design and Implementation (NSDI 20), Santa Clara, CA, USA, 25–27 February 2020; pp. 373–388.
9. Sun, X.; Kong, M.; Alkhazragi, O.A.; Telegenov, K.; Ouhssain, M.; Sait, M.; Guo, Y.; Jones, B.H.; Shamma, J.S.; Ng, T.K.; et al. Field demonstrations of wide-beam optical communications through water-air interface. *IEEE Access* **2020**, *8*, 160480–160489. [[CrossRef](#)]
10. Pompili, D.; Akyildiz, I. A cross-layer communication solution for multimedia applications in underwater acoustic sensor networks. In Proceedings of the 5th IEEE International Conference on Mobile Ad Hoc and Sensor Systems, Atlanta, GA, USA, 29 September–2 October 2008; pp. 275–284.
11. Domingo, M.C. Magnetic induction for underwater wireless communication networks. *IEEE Trans. Antennas Propag.* **2012**, *60*, 2929–2939. [[CrossRef](#)]
12. Qiao, G.; Muhammad, A.; Muzzammil, M.; Shoaib Khan, M.; Tariq, M.O.; Khan, M.S. Addressing the Directionality Challenge through RSSI-Based Multilateration Technique, to Localize Nodes in Underwater WSNs by Using Magneto-Inductive Communication. *J. Mar. Sci. Eng.* **2022**, *10*, 530. [[CrossRef](#)]
13. Hu, X.; Wang, D.; Lin, Y.; Su, W.; Xie, Y.; Liu, L. Multi-channel time frequency shift keying in underwater acoustic communication. *Appl. Acoust.* **2016**, *103*, 54–63. [[CrossRef](#)]
14. Watson, M.; Bousquet, J.-F.; Forget, A. Evaluating the feasibility of magnetic induction to cross an air-water boundary. *Int. J. Electron. Commun. Eng.* **2021**, *15*, 262–265. [[CrossRef](#)]
15. Tian, Z.; Zhang, X.; Wei, H. A test of cross-border magnetic induction communication from water to air. In Proceedings of the 2020 IEEE International Conference on Signal Processing, Communications and Computing (ICSPCC), Macau, China, 21–24 August 2020; pp. 1–4.
16. Ilyas, N.; Alghamdi, T.A.; Farooq, M.N.; Mehboob, B.; Sadiq, A.H.; Qasim, U.; Javaid, N. AEDG: AUV-aided efficient data gathering routing protocol for underwater wireless sensor networks. *Procedia Comput. Sci.* **2015**, *52*, 568–575. [[CrossRef](#)]
17. Zhu, S.; Chen, X.; Liu, X.; Zhang, G.; Tian, P. Recent progress in and perspectives of underwater wireless optical communication. *Prog. Quantum Electron.* **2020**, *73*, 100274. [[CrossRef](#)]
18. Jamali, M.V.; Mirani, A.; Parsay, A.; Abolhassani, B.; Nabavi, P.; Chizari, A.; Khorramshahi, P.; Abdollahramezani, S.; Salehi, J.A. Statistical studies of fading in underwater wireless optical channels in the presence of air bubble, temperature, and salinity random variations. *IEEE Trans. Commun.* **2018**, *66*, 4706–4723. [[CrossRef](#)]
19. Junejo, N.U.R.; Sattar, M.; Adnan, S.; Sun, H.; Adam, A.B.M.; Hassan, A.; Esmail, H. A Survey on Physical Layer Techniques and Challenges in Underwater Communication Systems. *J. Mar. Sci. Eng.* **2023**, *11*, 885. [[CrossRef](#)]
20. Enhos, K.; Demirors, E.; Unal, D.; Melodia, T. Software-defined visible light networking for bi-directional wireless communication across the air-water interface. In Proceedings of the 18th Annual IEEE International Conference on Sensing, Communication, and Networking (SECON), Virtual Conference, 6–9 July 2021; pp. 1–9.
21. Chen, L.-K.; Shao, Y.; Di, Y. Underwater and water-air optical wireless communication. *J. Lightw. Technol.* **2022**, *40*, 1440–1452. [[CrossRef](#)]
22. Tonolini, F.; Adib, F. Networking across boundaries: Enabling wireless communication through the water-air interface. In Proceedings of the SIGCOMM'18: Proceedings of the 2018 Conference of the ACM Special Interest Group on Data Communication, Budapest, Hungary, 20–25 August 2018; pp. 117–131. [[CrossRef](#)]

23. Tasadduq, I.A.; Murad, M.; Otero, P. CPM-OFDM Performance over Underwater Acoustic Channels. *J. Mar. Sci. Eng.* **2021**, *9*, 1104. [[CrossRef](#)]
24. Senne, J.; Song, A.; Badiy, M.; Smith, K.B. Parabolic equation modeling of high frequency acoustic transmission with an evolving sea surface. *J. Acoust. Soc. Am.* **2012**, *132*, 1311–1318. [[CrossRef](#)] [[PubMed](#)]
25. Qu, F.; Qian, J.; Wang, J.; Lu, X.; Zhang, M.; Bai, X.; Ran, Z.; Tu, X.; Liu, Z.; Wei, Y. Cross-medium communication combining acoustic wave and millimeter wave: Theoretical channel model and experiments. *IEEE J. Ocean. Eng.* **2021**, *47*, 483–492. [[CrossRef](#)]
26. Ma, D. Water Acoustics. In *Modern Acoustics Theory Foundations*, 1st ed.; Science Press: Beijing, China, 2004; pp. 65–68.
27. Lieshan, Z. Study on optical heterodyne detection technique of acoustic wave induced surface micro-waves. Ph.D. Dissertation, Harbin Institute of Technology, Harbin, China, 2017.
28. Dai, Z.; Sun, J.; Sui, P. Theoretical Study on the Water Surface Transversal Mini-wave due to the Underwater Sound Field. *J. Natl. Def. Univ. Sci. Technol.* **2004**, *26*, 95–118.

**Disclaimer/Publisher’s Note:** The statements, opinions and data contained in all publications are solely those of the individual author(s) and contributor(s) and not of MDPI and/or the editor(s). MDPI and/or the editor(s) disclaim responsibility for any injury to people or property resulting from any ideas, methods, instructions or products referred to in the content.